Indian Journal of Chemical Technology
Vol. 29, July 2022, pp. 339-353

Synthesis, crystal structure, quantum chemical calculations, electrochemistry and electro-catalytical properties as cytochrome P-450 model of tetradentate Mn(III)-Schiff base complex.

Lotfi Baameur[1], Djouhra Aggoun[*,1,2], Zakia Messasma[1,2], Gilles Bouet[3], Georges Le Guillanton[4], Jean Claude Daran[5] & Ali Ourari[1]

[1]Laboratoire d'Electrochimie, d'Ingénierie Moléculaire et de Catalyse Redox (LEIMCR), Faculté de Technologie, Université Ferhat ABBAS Sétif-1, Sétif, Algeria

[2]Département de chimie, Faculté des sciences, Université Ferhat ABBAS de Sétif-1, Sétif 19000, Algeria

[3]Laboratoire SONAS, EA 921, IFR149 QUASAV, Faculté de Pharmacie, 16 Boulevard Daviers, F-49045 Angers. Cedex 01, France

[4]Institut de Recherche Fondamentale et Appliquée, Université Catholique de l'Ouest, BP 10808. 49001 Angers Cedex 01, France

[5]Laboratoire de Chimie de Coordination du CNRS, 205 route de Narbonne, 31077 Toulouse Cedex 4, France

E-mail: aggoun81@yahoo.fr

Received 7 November 2021; accepted 22 May 2022

The tetradentate Schiff base ligand has been obtained from condensation with mixing ethylenediamine and 2 mmoles of 5-methoxy-2-hydroxybenzaldehyde in absolute ethanol H_2L. To the ethanolic solution was added manganese(II)acetate tetrahydrated and lithium chloride (LiCl) to obtain the tetradentate manganese(III) Schiff base complex [Mn(III)(Cl)L]. The prepared compounds have been characterized by several spectroscopic techniques such as elemental analyses, FT-IR, UV–vis., ^{1}H NMR and HRMS. In this paper, the X-ray diffraction (XRD) and the computational studies (DFT) of the ligand (H_2L) with its manganese(III)-Schiff base complex [Mn(III)(Cl)L] are described and confirmed the given molecular structures. The crystallographic studies have been utilized toelucidate the kinetics, selectivity and stereochemistry of the transferred oxygen atomsto the substrate molecules when the considered complex is used as catalyst according thecytochrome P450 model. In addition, the density functional theory (DFT) calculation with B3LYP/6-31G(d,p) level is performed to obtain the optimized geometries and electronic properties of the prepared compounds. The global reactivity parameters have also been calculated using the energies of frontier molecular orbitals suggesting that the ligand H_2L is more stable than its Mn(III) complex. This may be due to the presence of hydrogen bonds in the ligand and the weaker energies of coordination bonds in the complex. The electrochemical behaviour of Mn(III)(Cl)L has been studied by cyclic voltammetry in acetonitrile solutions at room temperature. The resulting cyclic voltammogram shows Mn(III)/Mn(II) couple at $E_{1/2}$= -0.62V with glassy carbon (GC) electrode. This redox couple is involved in the electrocatalytic cycle where the manganese(III) cation is successively mono-electronated until the formation of superoxo intermediates and then the oxo species, respectively. These oxo forms, generated in situ, transfer their oxygen atoms to the substrate giving the oxidized product. So, the chemical and electrochemical reactions, implicated in this electrocatalytical process, obey to the biomimetic oxidation reactions as those of monooxygenase enzymes (Cytochrome P450).

Keywords: Biomimeticoxidation, Cyclic voltammetry, Manganese Schiff base complex, Quantumchemical calculations, X-ray determination

In the past few years many reports have been devoted to the synthesis and characterisation of an important variety of Schiff bases as chelating agents[1,2]. This class of ligands were found to be of an easy handling and simple preparation since, they are currently obtained from phenolic and pyridinic compounds containing carbonyl functional group in their adjacent position when they are condensed on monoamino or diaminohydrocarbons in order to generate a suitable coordination sphere for synthesis of complexes of transition metals. Actually, these Schiff base complexes are extensively developed because of the wide variety of their versatile structures[3].

The increasing interest for transition metal complexes involving iminic ligands was inspired from their well-established catalytic efficiency neither in homogenous nor inheterogeneous catalysis or elctrocatalysis[4,5] with their wide range of biological activities such as antibacterial, antioxidant and antitumoral[6–8]. These compounds have been qualified to be the "working horse" owing to their ability for being readily subject to systematic modification of their electronic and steric properties.

During the last three decades, significant efforts have been made to design and synthesize Schiff bases and their corresponding complexes to apply them in several applications. Thus, the complexes of manganese, ruthenium and nickel with a wide variety of N_2O_2 and N_4 Schiff bases have been used as catalysts for hydrogenation, hydroformylation[9], carbonylation[10] and epoxidation reactions[11]. Furthermore, they play an important role in biological systems and are useful models for metalloenzymes such as mixed ligands of copper and nickel ions[12] and monooxygenase enzymes like NNOO tetradentate manganese(III)- or iron(III)-Schiff base complexes which are inspired from the porphyrinic complexes currently applied in mimicking the oxidation reactions in the being livings according the cytochrome P-450 model[13,14].

The Metallo-enzymes activating molecular dioxygen offer a roadmap to prepare novel transition metal complexes especially those of manganese and Iron that were designed essentially to the dioxygen activation chemistry[15-17]. By using these kinds of complexes, the chemistry of biomimetic model has been studied for a long time investigating different intermediates characterizing mechanisms withmolecular O_2 activation way[18,19]. These researches have been commanded to give valuable information about metal-oxo, metal-peroxo and other intermediates, even though the direct use of this oxidant remains relatively of a rare incidence[20-22].

Following the previous studiesof our recent investigations on the subject of the epoxydation of olefins such as cyclooctene and both isomers of stilbene using the same complex here in described as catalyst[23,24], we report the isolation andcharacterization of manganese(III) complex containing a Schiff baseligand, derived from the condensation of 5-methoxysalicylaldehyde with 1,2-diaminoethane (See Scheme 1).In addition, this complex was structurally characterized by singlecrystal X-ray diffraction, DFT andits electrochemistrystudy which is improved by an examination of some electronic parameters involved in the interactions between the metallic center and nature of substrate in the electrocatalytical system. So, this complex Mn(III)(Cl)L used in this study was prepared as reported in the literature[23]. The general procedure for the synthesis of the Schiff base ligand and its corresponding complex is illustrated by the Scheme 1.

Experimental Section

Physical measurements

All solvents and chemical are of reagent grade and were purchased from Aldrich and Fluka. They were used as received without any further purification. The solvents were dried before use with the appropriate drying reagents. Cyclic voltammetry experiments were carried out in an undivided Metrohm cell of 5 cm^3 using a TACUSSEL PRT (40-1X) potensiostat, an integrator IG–LN, a Kipp & Zonen X–Y recorder B.D 90. A planar, circular glassy carbon (GC) electrode (3 mm diameter) was employed as working electrode and a platinum wire as auxiliary (counter) electrode. All potentials are quoted with respect to the saturated calomel electrode (SCE). The solvent was acetonitrile with tetraethylammonium perchlorate (TEAP) as supporting electrolyte (ionic strength: 10^{-1} M). The electrodes were polished with diamond paste and rinsed with large amounts of acetone and finally with the usedsolvent. Controlled potential electrolyses were also recorded with a TACUSSEL PRT (40–1X) Potensiostat, an IG–LN Integrator, a Kipp & Zonen B.D 90 X–Y Recorder. The reference electrode (SCE) was separated from the working solution by a fine-porosity frit.

Electrocatalytic oxidation

All experiments for the electrocatalytic oxidation were carried out in 5 mL acetonitrile solutions containing TEAP (10^{-1} M), the complex catalyst (10^{-3} M), the axial base, 1- or 2-methylimidazole (10^{-2} M), benzoic anhydride (10^{-1} M) and hydrocarbon substrate (10^{-1} M). This mixture was placed in a Metrohm mono-compartment cell of 5 mL. Molecular oxygen was moderately bubbled into the electrolytic solution during the electrolysis. The selected electrolysis potential value was that of the maximum peak current (ip_c) at which the manganese-oxo species are massively

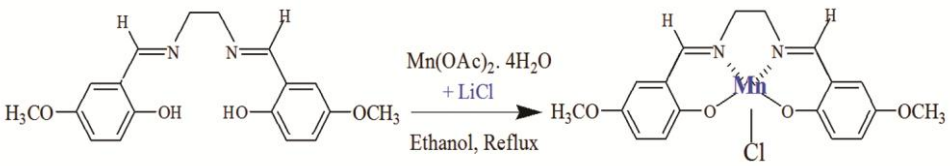

Scheme 1 — Preparation of the manganese(III) complex from tetradentate Schiff base ligand H_2L.

electrogenerated in situ. The electrolysis was then monitored by recording the peak current *ipc versus* time *ipc* = f(t) until reaching almost zero. During the electrolysis experiments, the consumption of the electricity was also determined by an integrator giving the charge passed through the cell.

X-ray Crystallography

A single crystal of Mn(III)(Cl)L, suitable for X-ray diffraction,was mounted under inert perfluoro-polyether on the tip of a loop and cooled in the cryostream of an Oxford-Diffraction XCALIBUR diffractometer. The structure was solved by direct methods using SIR 97[25]and refined by least-squares procedures on F_2 using SHELXL-97[26]. All H atoms attached to the C atoms were introduced at idealised positions and treated as riding on their parent atoms in the calculations. The drawing of molecule was produced with the program ORTEP-3[27]. All calculations were performed with the WINGX[28] suite of programs. Crystal data and refinement results are given in Table 1 and complete crystallographic results are further given as supplementary materials.

Table 1— Crystal data and structure refinement for Mn(III)(Cl)L.

Empirical formula	C_{18} H_{20} Cl Mn N_2 O_5
Formula weight	434.75
Temperature	180(2)
Wavelength	0.71073
Crystal system	Orthorhombic
Space group	P b c a
a (Å)	22.9532(16)
b (Å)	11.8861(6)
c (Å)	12.9769(8)
Volume (Å^3)	3540.4(4)
Z	8
ρ_{calcd} (g cm^{-3})	1.631
μ (mm^{-1})	0.931
F(000)	1792
Crystal size (mm^3)	0.12 x 0.12 x 0.03
θ range for data collection (°)	2.92 to 26.37
Reflections collected	19302
Reflections independent [R(int)]	3616 (0.078)
Completeness to θ_{max}(%)	99.9 %
Absorption correction	Multi-scan
Max./min. transmission	1.0 and 0.88877
Refinement method	F^2
Data / restraints / parameters	3616 / 3 / 252
Goodness–of–fit on F^2	0.820
R1, wR2 [$I>2\sigma(I)$]	0.0335, 0.0548
R1, wR2(all data)	0.0777, 0.0605
Largest diff. peak / hole (e.Å^{-3})	0.288 / -0.368

Computational details

This study reports computational studies on ligand H_2L and its Mn(III)(Cl)L complex. All calculations were performed by Gaussian 09 along with Gauss View 5.0.8 for visualizations. The geometries were fully optimized without any constraint on every bond length and bond angle. Geometry optimizations were conducted using the unrestricted DFT method using Beck's three parameter hybrid exchange functional[29], with Lee-Yang-Parr correlation functional (B3LYP) and 6-31 G (d, p) basis set[30,31]. The highest occupied molecular orbital (HOMO) and the lowest unoccupied molecular orbital (LUMO) were also performed under the same basic set. The reactivity descriptors that include energy gap (ΔEgap), ionization potential (IP), electron affinity (EA), hardness (η), softness (S), global electronegativity (χ) and electrophilicity (ω) have also been computed by the same approach as from our previous work[32]. The Molecular electrostatic potential (MEP) and Mulliken atomic charge were as well performed by the DFT.

Materials

The Mn(III)(Cl)L was prepared as reported by the literature[23]. 5-methoxysalicyaldehyde, 1,2-diaminoethane, $Mn(C_2H_3O_2)\cdot 4H_2O$, tetraethylammonium perchlorate (TEAP), benzoic anhydride, 2-methyl-imidazole (2-MeI), absolute ethanol and DMSO were purchased from Aldrich and used as received. For the supporting electrolyte, tetra-n-ethylammonium perchlorate (TEAP) was recrystallized in ethyl acetate and dried at 80°C in vacuum for 72 h. Traces of benzoic acid contained in the commercial benzoic anhydride were removed by simple washing by an aqueous solution (10 % w/w) of sodium hydrogenocarbonate ($NaHCO_3$) and recrystallized in a mixture of toluene/petroleum ether (40-60). Then, the product was abandoned in refrigerator overnight after that the solid was recovered by filtration, followed by washings with petroleum ether. Acetonitrile (analytical grade) was distilled over potassium permanganate (K_2MnO_4) and the distillate was received over 4 Å molecular sieves.

Synthesis

Synthesis of H_2L

Yellow coloured crystals of H_2L were synthesized by reacting 304 mg of 5-methoxysalicyaldehyde (2 mmol) which then added dropwise to 60 mg of 1,2-diaminoethane (1 mmol) in absolute ethanol (EtOH). This mixture is magnetically stirred and heated under

nitrogen atmosphere at 60°C for 30 min. A bright yellow product precipitated immediately. The solid obtained was recovered by filtration after washing with diethylether. The crude product was recrystallized from dichloromethane/acetone (95/5, v/v) by slow evaporation yielding 282 mg (86%). UV–Vis. (DMF) λ_{max}(n) (nm): λ_{max}(1) (345). FT-IR (KBr) νx (cm^{-1}): νC–OH (3600-3300), νC–H (aliphatic) (2916), νC=N (1637), νC=C (1578), νC–O (1275). ^{1}H NMR ($CDCl_3$) d (ppm): 12.715 (s, 2H, OH), 6.923-6.907(m, 4H), 8.325(s, 2H), 6.758, 6.751(2s, 2H), 3.960 (s, 4H), 3.772(s, 6H).

A single crystal of ligand (H_2L) was obtained by slow evaporation from an ethanol–methylene chloride (8/2, v/v) solvent mixture. The molecular geometry of H_2L with displacement ellipsoids drawn at the 50% probability level[33]; H atoms are represented as small spheres of arbitrary radii, and only the non-H atoms of the asymmetric unit are labeled.

Synthesis of Mn(III)(Cl)L

For the synthesis of the complex Mn(III)(Cl)L, 164 mg (0,5 mmol) of the ethanolic solution of ligand were placed in three necked flask equipped with condenser under nitrogen atmosphere. After that, 134mg (0,5 mmol) with an excess of 5% of manganese(II)acetate tetrahydrated ($Mn(OAC)_2{\cdot}4H_2O$) were slowly added to the previous solution of the ligand. The mixture was refluxed for one hour under nitrogen atmosphere and then foranother one hour under air atmosphere. 255 mg of LiCl were added to the mixture in order to exchange the acetate ions by chloride ones. So, the reflux is again maintained for 30 min after which, a partial removing of the solvent is performed and the solid is recovered by filtration. Thus, the complex was washed with small portions of cold mixture EtOH/MeOH (50/50, v/v), previously flushed with nitrogen at least for 20 min. Brown red crystals are collected and dried over P_2O_5yielding 58%. UV–Vis. (DMF) λ_{max}(n) (nm): λ_{max} (1) (355); λ_{max}(2) (437). FT-IR (KBr) νx(cm^{-1}): νC–OH (3500-3220), νC–H(aliphatic) (2939), νC=N (1637), νC=C (1541), νC–O (1278).HRMS (ESI) m/z: calcd. For $C_{18}H_{16}N_2O_4Mn[M]^+$ 381.32, found 381.4.

Results and Discussion

The newly synthesized manganese complex was stable at atmospheric temperature and pressure. It was insoluble in organic solvents like methanol and ethanol while is soluble in coordinating solvents such as DMF, DMSO and acetonitrile.

Spectral characterization

UV–visible spectra

The UV–visible spectra of the ligand and its manganese(III) complex were carried out in DMF solutions. The Schiff base ligand H_2L shows a broad absorption bandat 345 nm, attributed to n–π* transitions involving the conjugated system of the complex with azomethine groups. This absorption band displays a shifting to the higher frequencies after coordination (situated at 355nm). The absorption spectrum of Manganese(III)-Schiff base complex shows an intense charge transfer at 437 nm suggesting a distorted octahedral arrangement around the metallic centre like manganese(III)[34].

FT-IR spectra

The FT-IR spectrum of H_2L exhibits a broad band in the range of 3600-3300 cm^{-1} characteristic of the intramolecular hydrogen bonding due to thephenolic functional groups (υOH)[35]. Moreover, another important absorption band is the azomethine group ($\upsilon_{C=N}$) appearing at 1637 cm^{-1}. Ether bands (υ_{C-O}) were as well observed at 1275 cm^{-1} while those belonging to the aromatic rings ($\upsilon_{C=C}$) absorb at 1578 cm^{-1}. For the spectrum of the complex, it shows a broad ranging from 3500 to 3220 cm^{-1}, characterizing the presence of hydroxyl groups (υ_{OH}) indicating the presence of water traces. These absorption bands were consistent to the presence of water molecules in the lattice crystal since the OH bonds should be disappeared to the benefit of the O-Mn bonds obtained after coordination of manganese ions with the phenoxy groups. Regarding the azomethine absorption band ($\upsilon_{C=N}$), it was observed at the same frequency 1637 cm^{-1} of the ligand without showing any shifting. This is, probably, due to the higher σ-donor effect of the methoxy groups compensating the loss of the electronic density around this bond after coordination. As for the ether groups (υ_{C-O}), they absorb at 1278 cm^{-1} showing a slight increasing of this frequency due to strengthening of the electronic density of the considered bond[36]. Finally, the double bonds of the aromatic rings ($\upsilon_{C=C}$) shift from 1578 to 1541 cm^{-1} suggesting a significant bathochrome effect, due to an important improvement of the electronic delocalization passing through metallic ion[37]. The coordination of Mn^{II} ions to the ligand molecules is confirmed with υ_{PhO-Mn} bonds[38], observed in the far-red region at 482 cm^{-1}. These results are in good agreement with the structure of the expected compound and the results reported in the literature[39].

^{1}HNMR spectrum

The protons NMR characteristics of H_2L are given according their different protonic environments, characterized by their ownchemical shifts (δ, ppm). However, the phenolic protons (OH) of the ligand, appearing at 12.715 ppm, are strongly deshielded to the weak fields, due to their interactions with nitrogen atoms of the azomethine groups. This phenomenon is well known in NMR theory, namely with 2-hydroxyacetophenone, largely discussed in NMR theory, where the proton of its hydroxyl group resonates at 12.05 ppm, shifting downfield than the phenol proton, usually observed at 7.54 ppm[36]. For the aromatic protons are rather characterized by two distinct protonic environments (H_2,H_3) and H_5. The former resonate as multiplet between 6.923 and 6.970 ppm while the latter H_5 are observed as two singlets at 6.758 and 6.751 ppm respectively. The H_4 protons, representing the both methoxy groups, give a singlet at 3.772 ppm. As for the protons H_7, belonging to the molecular residue of ethylenediamine (-$[CH_2]_2$-), they resonate at 3.960 ppm while those azomethine groups (-N=CH) H_6 were observed at 8.325 ppm seeing that they are situated in the deshielding zone of the electrons circulation of aromatic ring and azomethine group.

Mass spectrum

The mass spectrum obtained corroborates perfectly with the molecular mass of manganese(III)-Schiff base complex ($M^{\cdot+}$) m/z 381.4 without its chloride anion, seeing that it was analyzed using the technique, involving fast atom bombardment in the positive mode (HRMS (ESI)). This molecular peak was also accompanied by two other peaks, attributed to the protonated forms at ($M^{\cdot+}$ + $1H^+$) m/z 382.4 and (ii) ($M^{\cdot+}$ + $2H^+$) m/z 383.4 while a third one, appearing at 412.4, it corresponds to [$M^{\cdot+}$ + CH_3O^-] m/z (381.4 + 31) where the molecule of methanol is found to be associated.

Crystal structure

The manganese complex was also characterized by X-ray diffraction, and the ORTEP representation with the atomic numbering are given in Fig. 1(a). The crystallographic data and structure refinement summary for thecomplex Mn(III)(Cl)L are listed in Table 1. The selected Bond lengths [Å] and angles [°] for this complexwere presented in Table 2 and 3, respectively.

The Mn atom of the Mn(III)(Cl)L complexadopts a pseudo-octahedral geometry with the tetradentate OONN Schiff base occupying the equatorial plane whereas a water molecule and a Cl atom are located in the axial positions [Fig. 1(a)]. This structure is

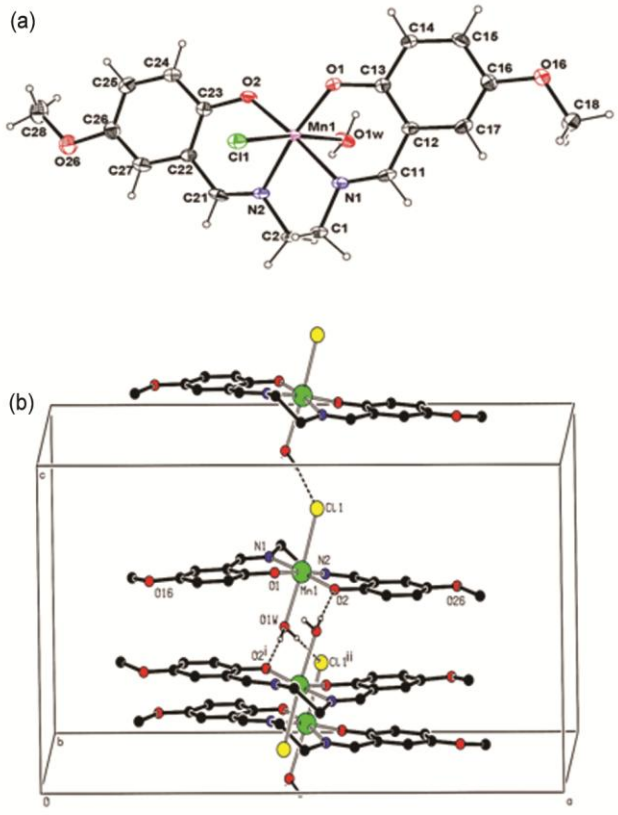

Fig. 1 — (a) X-ray molecular structure of Mn(III)(Cl)-L with its atomic numbering scheme. Ellipsoids are drawn at the 30% probability level. H atoms are represented as small sphere of arbitrary radii; (b) Packing of molecules showing the O-H…Cl and O-H…O interactions resulting in the formation of chains parallel to the c axis and layers parallel to the (1 0 0) plane.

Table 2— Hydrogen bonding parameters.

	D – H(Å)	H...A(Å)	D...A(Å)	D - H...A(°)	Symmetry code
O1W- H1W… O2	0.8400	2.0100	2.849(2)	174.00	1-x, -y, 1-z
O1W- H2W… Cl1	0.8500	2.3700	3.1921(17)	164.00	X, -y+1/2, z-1/2
C18- H18B… Cl1	0.9800	2.7900	3.549(3)	134.00	x-1/2, y, 3/2-z
C28- H28C… O16	0.9800	2.4800	3.425(3)	161.00	1-x, -y, 1-z
C18- H18A… Cg2	0.98	2.54	3.399(3)	146	x-1/2, y, 3/2-z
C28- H28A… Cg1	0.98	2.78	3.667(3)	151	½+x, y, 3/2-z

Table 3 — The calculated and experimental values of the bond lengths and bond angles of compounds H_2L and Mn(III)(Cl)L.

	H_2L			Mn(III)(Cl)L	
	X-ray	B3LYP		X-ray	B3LYP
Bond lengths (Å)			Bond lengths (Å)		
C2-N2	1.47	1.455	Mn-Cl	2.16	2.5606
C1-C1^{i}	1.54	1.515	Mn-O1w	2.3163	2.2147
C1-H1A	1.07	0.97	Mn-O1	1.8144	1.8635
C1-H1B	1.07	0.97	Mn-O2	1.8316	1.8853
C3-N2	1.2936	1.275	Mn-N1	2.7289	1.974
C3-C4	1.54	1.456	Mn-N2	2.725	1.9855
C3-H3	1.07	0.93	N1-C1	1.276	1.49
C4-C9	1.4014	1.405	N2-C2	1.473	1.4941
C4-C5	1.4014	1.408	O1-C13	1.328	1.4758
C5-O5	1.43	1.350	O2-C23	1.341	1.4618
C5-C6	1.4014	1.391	O16-C18	1.429	1.43
C6-C7	1.4014	1.366	C12-C17	1.400	1.3955
Bond angles (°)			Bond angles (°)		
N2-C1-C1^{i}	109.4712	109.99	O1-Mn-N1	82.9722	91.99
N2-C1-H1A	109.4713	109.7	O1-Mn-N2	124.2351	171.53
C1^{i}-C1-H1A	109.4712	109.7	O2-Mn-N1	155.481	172.37
N2-C1-H1B	109.4713	109.7	O2-Mn-N2	90.3434	91.78
C1^{i}-C1-H1B	109.4712	109.7	O1-Mn-O1	111.5283	94.33
H1A-C1-H1B	109.4713	108.2	N1-Mn-N2	65.2046	81.50
N2-C3-C4	120.0	121.80	C11-N1-C1	121.1	127.2925
C9-C4-C5	120.0	119.26	C11-N1-Mn	125.60	115.9734
O5-C5-C6	120.0	119.26	C21-N2-Mn	125.09	126.0647
O5-C5-C4	120.0	121.64	C2-N2-Mn	114.06	116.0765
C5-C6-H6	120.0	119.6	C23-O2-Mn	127.32	121.9562

closely related to the reported structure of [MnCl($C_{16}H_{12}Cl_2N_2O_2$)(H_2O)], the difference being the substituents in para position, methoxy for the structure presented here and Cl atom for the reported one.

The occurrence of O-H…Cl hydrogen bonds built up an infinite chain parallel to the c axis [Fig. 1(b)]. The second H atom of the water molecule is involved in a O-H…O(2) hydrogen bond linking the chains to form a layer parallel to the (1 0 0) plane. Moreover, the O-H…O interactions result in the formation of a $R_2^2(8)$ graph set motif[40].

DFT Calculations

Molecular geometry

The optimized structures of the compounds H_2L and Mn(III)(Cl)L are presented in Fig. 2. The bondlengthsand bond angles of the compounds computed at the B3LYP/6-31G(d,p) level of theory by using Gaussian 09 are summarized in Table 3. The theoretical and experimental bond distances and bond angles of ligand H_2L and its Mn(III)(Cl)L complex are in good agreement. There appear small discrepancies between experimentally determined and computed bond lengths and angles in Table 3. For H_2L, C-C bond distances are almost 1.40 Å; C-C1^{i} and C-H bond distances are 1.54 and 1.07Å, respectively. The C2-N(2) and C3-N(2) bond distances are 1.46, 1.28 Å, respectively. For complex Mn(III)(Cl)L, Mn-O(1) and Mn-O(2) bond distances are 1.82 Å approximately and the average of Mn-N(1), Mn-N(2) bond distances are 2.72 Å. The biggest difference between experimental and theoretical bond length arises withMn-N(1) (0.75 Å) and Mn-N(2) (0.73 Å).In fact, they should really not be the same due to the approximations in the DFT level and the different physical meaning of the X-ray and computed parameters. The physical meaning of experimental bond lengths depends on the physical techniques used in their determination. Also, there is another possible source of difference between experimental and theoretical results when they refer to different physical states[41].

Frontier Molecular Orbitals

In order to provide get a better understanding of the frontier molecular orbital energies (HOMO and

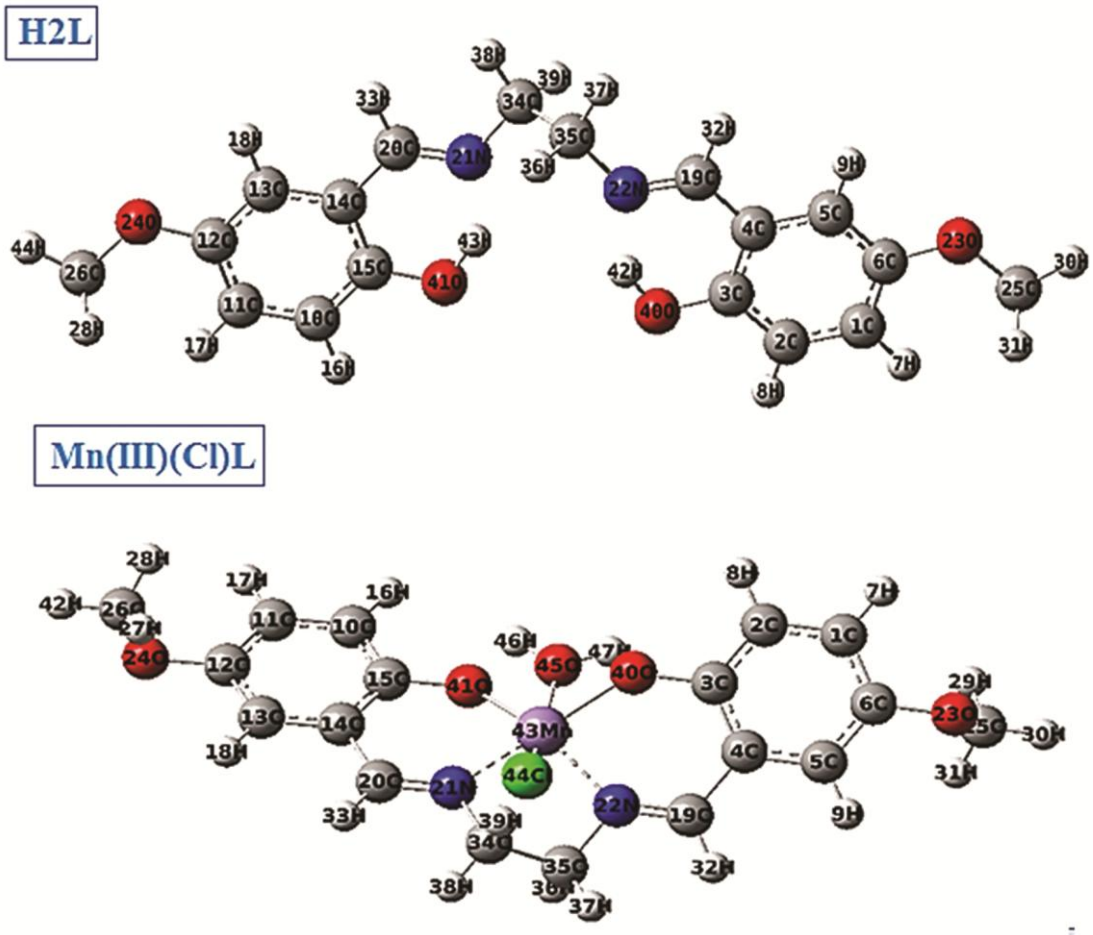

Fig. 2 — Optimized structures of compounds H_2L and Mn(III)(Cl)L.

LUMO), B3LYP hybrid function by the Gaussian 09 using a DFT method has been accomplished. In addition, HOMO and LUMO are very useful quantum chemical parameters to assess the molecules reactivity and are used to measure other parameters such as ionization potential (IP), electron affinity (EA), electronegativity (χ), chemicalpotential (μ), chemical hardness (η), molecular Softness (S) and electrophilicity index (ω). These estimators are vital parameters of quantum chemistry. The theoretical results concerning the ligand H_2L and its Mn(III)(Cl)Lcomplex are listed in Table 4. This information refers to better illustrate the optimized structure of the investigating compound. The isodensity surface plots of HOMO and LUMO forH_2L and Mn(III)(Cl)L are shown in Fig. 3. As itcan be seen in this figure, the electron density of the Mn(III)(Cl)L complex is mainly distributed over the nitrogen, oxygen and Mn atoms for both HOMO and LUMO. In the Table 4, the HOMO–LUMO energy gap of the ligand H_2L and its Mn(III)(Cl)L complex are 3.8406 eV and 1.3937 eV, respectively. The given low energy gap (1.3937 eV) indicates ahigh reactivity of the complex due to the easy charge transfer process[42]. The nucleophilicity and electron-

Table 4 — Summary of theoretical results obtained for optimized geometries of compounds H_2L and Mn(III)(Cl)L using DFT method.

	H_2L	Mn(III)(Cl)L
E_{HOMO}(eV)	-5.3284	-3.6875
E_{LUMO}(eV)	-1.4851	-2.2937
E_{HOMO-1} (eV)	-5.3448	-4.3090
E_{LUMO+1} (eV)	-1.3246	-1.8865
E_{HOMO}- E_{LUMO}(eV)	3.8406	1.3937
$\mu_{D,}$ (Debye)	4.7181	4.7181
IP (eV)	5.3284	3.6875
EA (eV)	1.4851	2.2937
χ (eV)	3.4054	2.9906
μ(eV)	3.4054	-2.9906
η (eV)	1.9203	0.6968
S (eV)	0.2637	0.7175
ω(eV)	3.0192	6.4172

IP = $-E_{HOMO}$, EA = $-E_{LUMO}$, $\chi = -(E_{LUMO}+E_{HOMO})/2$,
$\mu = 1/2(E_{HOMO} + E_{LUMO})$, $\eta = 1/2(E_{LUMO}-E_{HOMO})$,
$s = 1/2\eta, \omega = \mu^2/2\eta$.

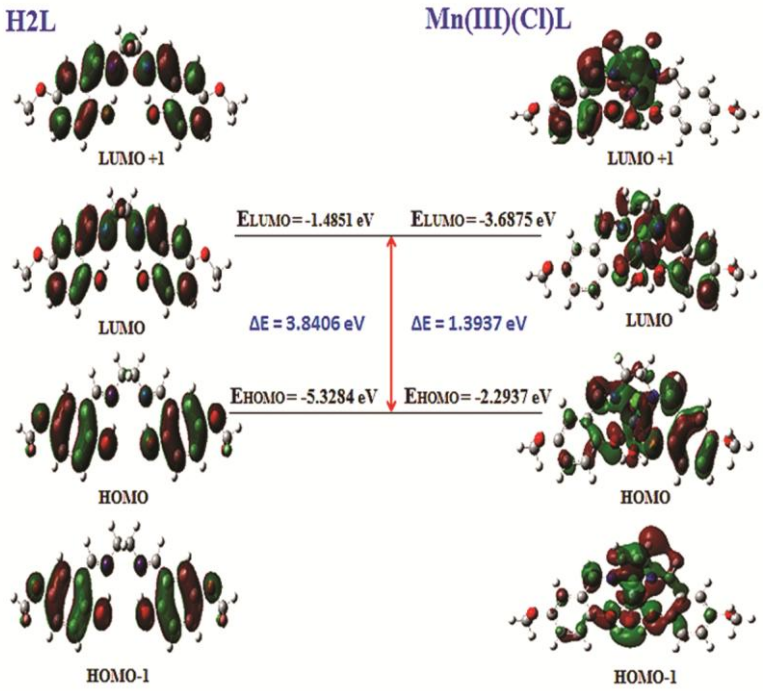

Fig. 3 — DFT molecular orbital diagrams of LUMO and HOMO spin of H_2L and Mn(III)(Cl)L.

withdrawing ability of a compound may beestimated through ionization potential (IP) and electron affinity (EA), respectively[43]. These quantities derived from E_{HOMO} and E_{LUMO}, respectively reflect the nucleophilic properties and electron attraction power (Table 4). The low value of hardness (0.6968) indicates that alower energy is needed for electron transition from HOMO to LUMO which means that the complex is susceptible to deform and denote the potential ease of reactivity in this compound. So, we can measure the electrophilic power of molecules by global electrophilicity indices (ω)[44]. Therefore, a molecule with a high electrophilicity index should be exhibit an electrophilic behaviour. The electrophilicity of the ligand H_2L and that of its Mn(III)(Cl)L complex are 3.0192 eV and 6.4172 eV, respectively. We noticed lower electronegativity (χ) power for the complex (Table 4), which is tenable due to the positively charged coordinating metal (Mn).

Molecular electrostatic potential (MEP)

The molecular electrostatic potential (MEP) has been used as a useful method in research of molecular structure with its physicochemical property relationship. It is also applied for predicting sites, relative reactivities towards electophilic and nucleophilic sites and to investigate in the studies of biological identification as well as hydrogen bonding interactions[45]. The electrostatic potential at the surface are represented by different colours, and the colour code of these maps is in the range from -0.038a.u. (deepest red) to 0.038 a.u. (deepest blue) for ligand H_2L and in the range from -0.0425 a.u. (deepest red) to 0.0425 a.u. (deepest blue) for Mn(III)(Cl)L complex. The color scheme for the MEP surface is red (electron-rich or partially negative charge), blue (electron-deficient or partially positive charge), light blue (slightly electron-deficient region), yellow (slightly electron-rich region), respectively. The MEPs contour maps of ligand H_2L and its Mn(III)(Cl)L complex are illustrated in Fig. 4(a). As itcan be seen, the regions having the most negative potential are mainly localized over the nitrogen atom from C=N bond attached to benzene ring followed by the oxygen atom from hydroxyl group in a molecule, those having the most positive potential are over the hydrogen atoms. For the H-atoms, they have showed a positive potential region in these structures. While the hydrogen atom bonding with oxygen atoms possesses large positive potential, due to the electronegativity of oxygen atoms. These negative and positive sites in these molecular structures help to localize the zones where the electrophilic and nucleophilic sites should previously be determined[46].

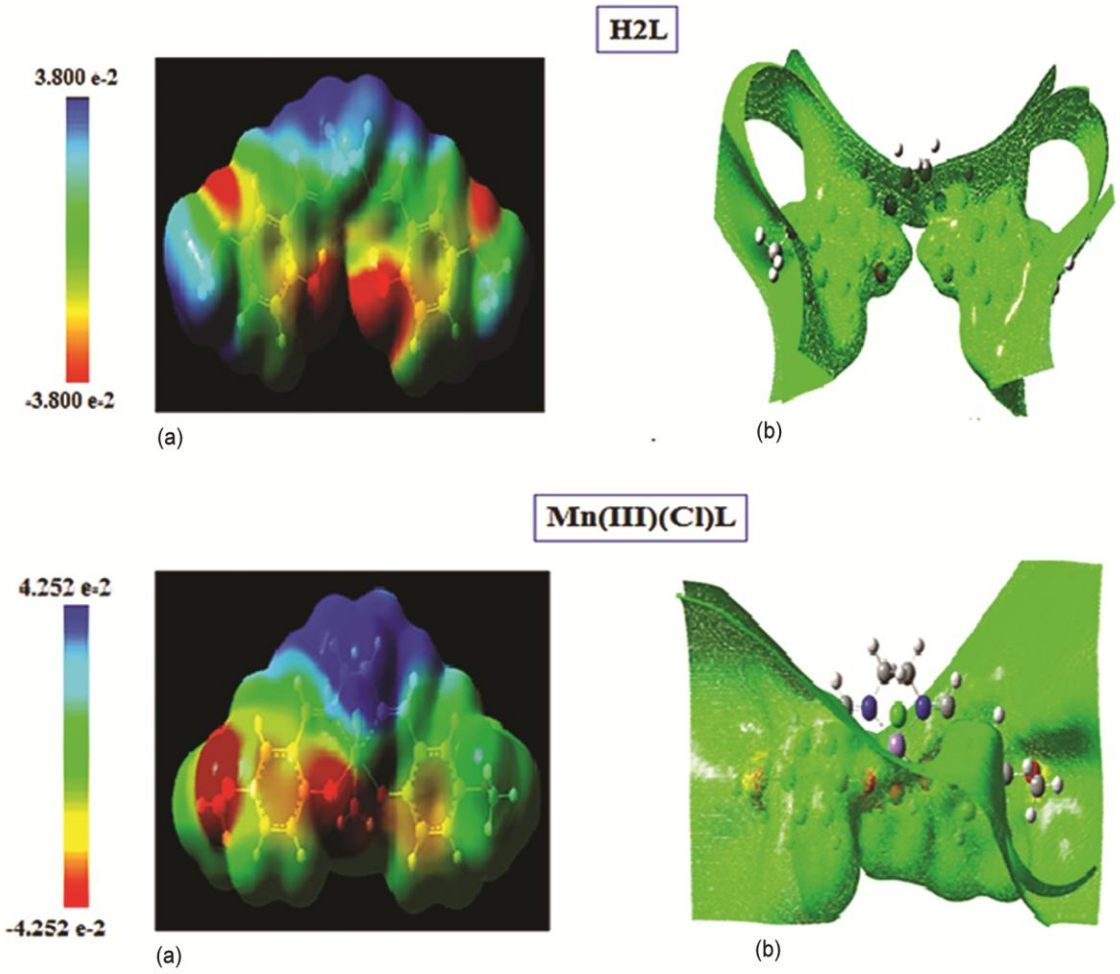

Fig. 4 — Molecular electrostatic potential surface (a), electrostatic potential (b) for H_2L and Mn(III)(Cl)Lobtained at B3LYP/6-31G(d,p).

Electrostatic potential (ESP) is illustrated in Fig. 4(b) to confirm the most negative and reactive sides like oxygen and nitrogenatoms.

Mulliken Atomic Charges

The distribution of electric charge on the molecules plays a crucial role taking into account of the following factors such as electrostatic potential, dipole moment, vibrational spectroscopy as well as acid-base properties and so on[47,48]. According to Fig. 5, it reveals the atomic charges assignment in molecules, the Mulliken atomic charges were calculated at the level of B3LYP/6–31G(d,p) theory in this figure. For the ligand H_2L, it showed that theC3, C6, C12 and C15 are the most positive charge and O23, O24, O40, O41, N21 and N22 have the most negative charge. So, it is observed that the most nucleophilic centers are those of oxygen and nitrogen heteroatoms which having the most electrophilic susceptibility. The positively charged centers are the most susceptible sites for the nucleophilic attacks i.e.as the electron donation. However, the most negatively charged centers are the most susceptible sites for electrophilic one[49]. All hydrogen atoms have slight amount of positive charges except for hydrogen atoms of hydroxyl groups with higher positive charge. For the Mn(III)(Cl)Lcomplex, the most positive charge is found to be uniformly distributed on the surface sphere of Mn(III) ion, as it would be expected. Considering that the oxygen and nitrogen atoms have negative charges, the coordination environment around metal center would be understood. The C3 and C15 atoms have higher positive charges than the other C atoms due to the coordination of electronegative O atoms. The hydrogen atoms have positive charges while the carbon atoms have either positive or negative charges.

As for the Mulliken atomic charges of the ligand H_2L and its Mn(III)(Cl)L complex, they are estimated

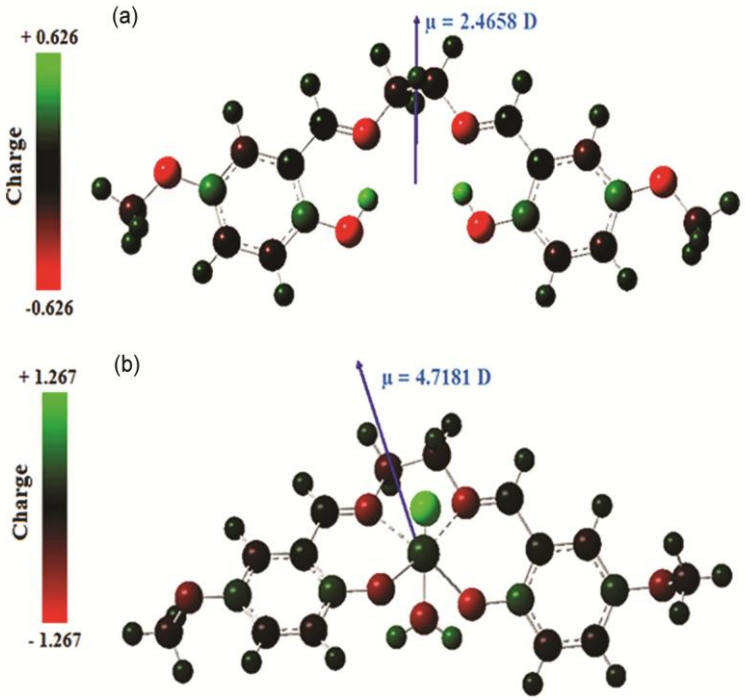

Fig. 5 — Atomic charges distributions along with dipole moments for the investigated compound; computations performed at the level of DFT theory (B3LYP 6–31G(d,p): (A)H_2L; (B)Mn(III)(Cl)L.

and calculated by DFT using B3LYP 6-31G (d,p) at a basis set.

Electrochemical study of the Mn(III)(Cl)L complex in the catalytic conditions

The activation of small molecules such as NOx, CO_2 and O_2[50] is an attracting area of research essentially applied in catalysis, electrocatalysis and sensors. In organic media, the electro-assisted of biomimetic reactions involving molecular oxygen and those developing another reactant like electron (electrochemical methods) offer simple recycling of the catalyst without any change in its molecular structure. Nowadays, these methods develop an intense rise in its activity since, they are frequently reported in the literature. In this case, we will briefly describe the activation of molecular oxygen by this manganese(III)-Schiff base complex Mn(III)(Cl)L. So, this is a catalytic system functioning according the cytochrome P450 model. The electrochemical behaviour of the Mn(III)(Cl)L complex has been studied in acetonitrile solution by employing cyclic voltammetry (CV) with a glassy carbon electrode (GC) containing 0.1 M TEAP. The cyclic voltammogram of the manganese complex display two systems located at $E_{1/2}$=-0.62Vand $E_{1/2}$= +0.56 V attributed to the Mn(III)/Mn(II)and Mn(III)/Mn(IV) couple, respectively. Hence, we have investigated the effect of the peak currents (i_{pa} and i_{pc}) versus scan rate for the redox systems of Mn(III)/Mn(II) onto, the GC electrode. It can be seen from this figure that the redox current increases with the increase of scan rate and the anodic wave shifts towards the more positive potential values whereas the cathodic wave shifts rather towards the more negative potentials as the scan rate increases. Consequently, this Mn(III)/Mn(II) system seems to obey to a diffusion controlled described by Nicholson's theory[51].

The cyclic voltammetry study of the complex Mn(III)(Cl)L, under dinitrogen atmosphere, exhibits a well-defined redox system of Mn(III)/Mn(II) as expressed by the following equation 1 and Fig. 6 (curve 1).

$$\text{L-Mn(III)} + 1e^- \leftrightarrow \text{L-Mn(II)} \quad \ldots(1)$$

After addition of the axial base like 2-methylimidazole, it allows to obtain a well-defined redox system Mn(III)/Mn(II) (Fig. 6, curve 3) with which, i_{pa} and i_{pc} peak currents become more sharper than those previously recorded in curve 2.

When the dioxygen is introduced in the solution of reaction mixture, it reacts chemically with Mn(II)

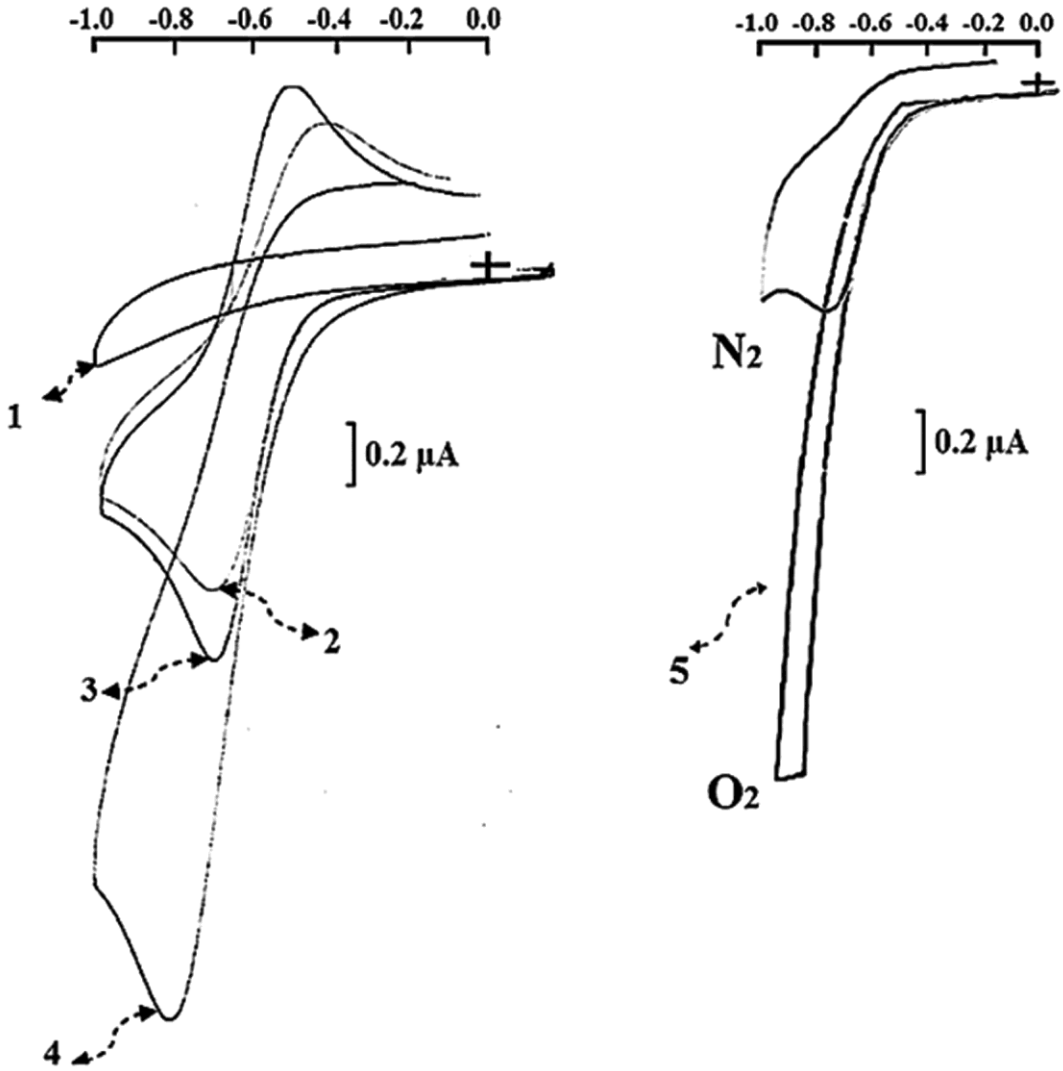

Fig. 6 — Voltammograms characterizing different electro-active species involved in the catalytic oxidation reaction according cytochrome P450 model, (1) Electrolytic solution without complex with 0.1M TEAP in CH_3CN, (2) Same conditions in (1) with addition of 1 mM Mn(III)(Cl)L under N_2 atmosphere, (3) Same conditions in(2) with addition 10^{-2}M of 2-MeIm, (4) Same conditions in (3)working under O_2 atmosphere,(5) Same conditions in (4) with addition 10^{-2} M of benzoic anhydride.

species after removing all dinitrogen molecules as indicated by the following equation 2.

$$L\text{-}Mn(II)\text{-}L + O_2 \leftrightarrow L\text{-}Mn(III)\text{-}O\text{-}O^{\cdot} \quad ...(2)$$

In these catalytic conditions, the dioxygen is activated owing to the presence of manganese complexacting as catalyst. This dioxygen activation leads to the formation of super-oxo species according the equation 2 above mentioned and evidenced by the Fig. 6 (curve3). A second electron is again transferred to the super-oxo species as shown by the following equation 3.

$$L\text{-}Mn(III)\text{-}O\text{-}O^{\cdot} + 1e^{-} \leftrightarrow L\text{-}Mn(III)\text{-}O\text{-}O^{-}eq \quad \ldots(3)$$

In this case, the reduction wave corresponding to the i_{pc} of the redox system of Mn(III)/Mn(II) increases while the i_{pa} peak current decreases until to its almost total disappearance. This is due to the consumption of the total Mn(II) species avoiding their re-oxidation process[52] as it can be observed on the Fig. 6 (curve 2). Furthermore, the both successive electronic transfers (eqs. 1, and 3) occur at the same potential generating, in situ, the oxygenated species above mentioned. This electrochemical mechanism was sufficiently discussed in the literature but, unfortunately, it remains not definitively established[53].

However, the addition of an electrophile agent to the reaction medium such as benzoic anhydride allowsto cut the O-O bond leading to the formation of metal-oxo species accompanied with two benzoate anions as below summarized by the equation 4.

$$L\text{-}Mn(III)\text{-}O\text{-}O^{-} + (PhCO)_2 \rightarrow L\text{-}Mn(V)=O + 2PhCOO^{-} \quad \ldots(4)$$

These manganese-oxo species are thus formed at the same potential as previously indicated for the super-oxo ones[54] as it can be seen on the Fig. 6 (curve 5). So, the electrocatalytic current is judged from the ratio $i_{pc}O_2/i_{pc}N_2$. This ratio is equal here to 3.90, approaching almost four times the i_{pc} peak current obtained under nitrogen atmosphere. Moreover, it must as wellnotice that these oxidant moieties currently used in the epoxidation or oxidation processes of hydrocarbons such as olefins and alkanes, respectively. Finally, these oxidation reactions may be illustrated by the fifth following equation 5, summarizing the oxidation reactions occurring in the being livings according the cytochrome P450 model[55].

$$L\text{-}Mn(V)=O + S(substrate) \rightarrow SO + L\text{-}Mn(III) \quad \ldots(5)$$

The formation of these oxidant species L-Mn(V)=O constitutes a crucial step of the electrocatalytic cycle, seeing that if their oxygen atoms are transferred to the substrate molecules (S), the oxidized product (SO) is consequently formed with an efficient turnover but, when they are electro-reduced according to the following equation 6, the resulting turnover becomes not efficient and the oxidized product (SO) not obtained.

$$L\text{-}Mn(V)=O + 2e^{-} \rightarrow 1/2O_2 + L\text{-}Mn(III) \quad \ldots(6)$$

Therefore, the catalyst is regenerated to initiate a new electro-catalytic cycle as above summarized in Scheme 2.

In fact, this complex Mn(III)(Cl)Lwas early studied as catalyst in the epoxidation of cyclooctene to its corresponding cyclooctene oxide[56]. This electrocatalysis study revealed that this epoxidation reaction is totally inefficient since, the cyclooctene oxide was not detected even at the traces state whereas, when it was used for the epoxidation of the two stilbene isomers, an acceptable yields of epoxystilbene isomers (Z,E) were obtained in the same experimental conditions[24]. In this case, it must note that Kochi *et al.*[57] were the first pioneers of this study focusing the epoxidation reaction using iodosylbenzene (chemical method) as donor of oxygen atoms with the same catalysts differently substituted with methoxy groups. These authors concluded that this chemical catalysis is very poor particularly when the methoxy (CH_3O-) is fixed on

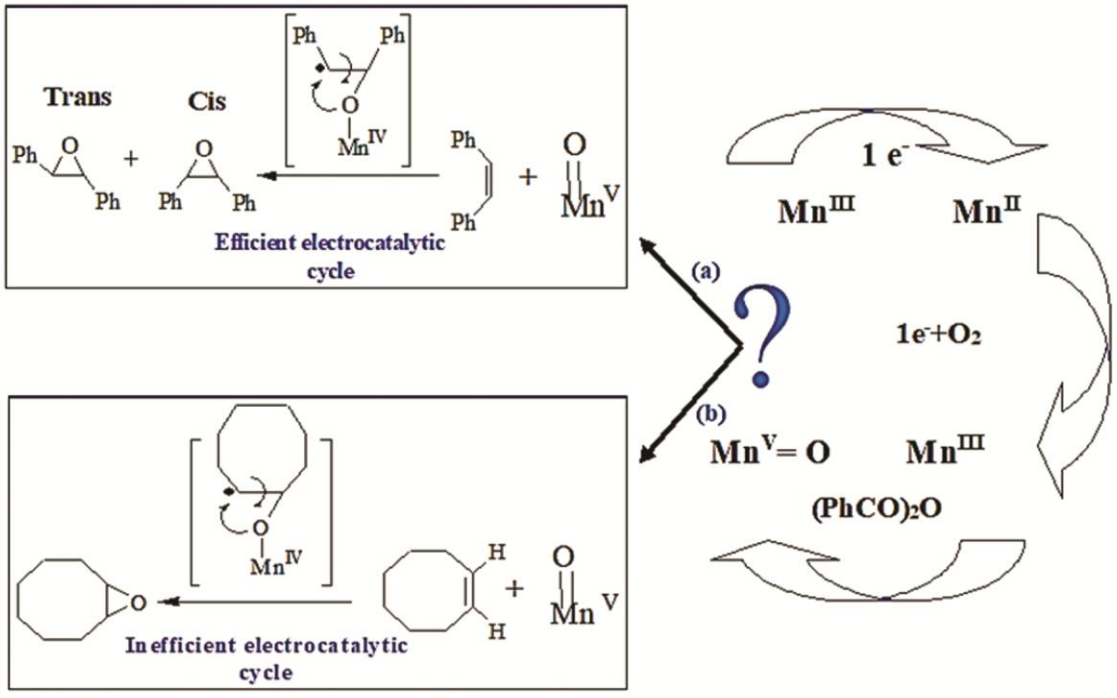

Scheme 2 — Catalytic cycle summarizing the oxidation reactions according the cytochrome P450 model.

the position five (5-CH_3O salicylaldehyde) as above mentioned. This result may be attributed to the strong electrodonor effect of the both methoxy groups playing a role compensating the loss of the positive charge on the metallic center (manganese ion) since, as the electropositive charge decreases on the metal center the electro-catalytic efficiency of the epoxidation reaction automatically decreases.The electrocatalytic behaviours of this catalyst seems to be similar to the most catalytic studies commonly known in the literature where each catalytic system may be considered as a separate catalytic system. So, in the case of the epoxydation of cyclooctene, the metal-oxo species seem to be preferentially and totally electroreduced to the initial form of the catalyst Mn(III)(Cl)L since the epoxidic product was not detected even as traces sate.

Regarding the epoxydation of the both stilbene isomers[24], it was observed that there is an epimerisation resulting from a relative stabilization of the reactional intermidiates which are essentially caused by an inducing of an excess of electronic density from the both methoxy groups on the metallic centre. The increase of the electronic density on the metal ion causes an increasing in its stability and induces as well longer life time for the considered reactional intermidiates which, therefore, allow the rotation around the σ-bonds leading to the formation of the two isomers epoxy Z-stilbene and E-stilbene (epimerisation).

The epoxidation reaction of trans-stilbene (See Scheme 2, way a) with manganese oxo species passes through one step for which the reactional intermediate is stabilized by a donor mesomere effect using the delocalized aromatic system presenting a sp^2 hybridization (Phenyl group) which induces a stronger electronic density on the metallic center. Therefore, the stabilization of this intermediate increases its life time allowing it to rotate around the sigma bond causing an epimerization reaction and a splitting C-C σ-bond of the ethylenic system leading to the formation the both isomers cis and trans and Benzaldehyde, respectively[58,59]. This behaviour was only observed in the electroepoxidation of the cis-isomer while, the trans-isomer provides practically the trans-epoxystilbene (Reaction without epimerization).

For the second way b, the attach of the cyclooctene molecules by the oxidant intermediates such as manganese-oxo seem to be not efficient because their interactions are weaker since, the cyclooctyl group with its sp^3 hybridization cannot stabilize sufficiently the resulting reactional intermediate and consequently, if we consider an equilibrium between the two molecular forms, it is found to be almost practically shifted to initial reagents where the manganese-oxo species are totally electroreduced to the initial form of the catalyst seeing that the cyclooctene oxide was not detected even as traces state[23].

Conclusion

As conclusion of this work, the molecular structures of the tetradentate Schiff base ligand H_2L and its corresponding manganese(III) complex Mn(III)(Cl)Lhave been synthesized and characterized. These molecular structures were finally evidenced by the mass spectrometry and also by single crystals of the ligand and its corresponding manganese(III) complex using crystallographic determinations. Geometry of the ligand and its complex is fully optimized using the valuable DFT methods. The computed structural parameters are in agreement with the experimental data, confirming validity of the optimized geometry for the Mn(III) complex. In the investigated octahedral complex, the ligand H_2L is a dianionic tetradentate ligand, which coordinates to the Mn metal ion in a N,N,O,O manner. The O1 and O2 phenolic oxygens together with the azomethine nitrogens (N1, N2) occupy four coordinative positions of the square plane of the octahedral complex. Two axial positions of the octahedral complex have been occupied by a molecule of water and one atom of Cl. These axial positions are deliberately occupied by nitrogen bases such as 1- or 2-methylimidazole playing the role to extract the metallic center from its own plane in order accelerate its nucleophilic attack as the molecule of dioxygen (O_2).The small HOMO-LUMO energy gaps are the main indicators of charge transfer interaction taking place in the complex. Additionally, H_2L has been found to be more stable (chemically hard) in gas phase than the solid one of thiscomplex. This manganese(III) complex was studied by cyclic voltammetry with which its electrocatalytical properties were well discussed for the olefins epoxidation reaction and hydrocarbons oxidation. In this case, the octahedral geometry of Mn(III) complex could elucidate the course of the catalytic reactions involved in its different possible geometrical configurations. Thus, it seems that this complex may adopt a configuration rendering it more

efficient to catalyse the epoxidation reactions of stilbene isomers than cyclooctene in spite of its lower steric hindrances around its ethylenic system.

Acknowledgements

The authors thank the Algerian Ministry of Higher Education and Scientific Research (MESRS) and the Director General for Scientific Research and Technological Development (DGRSDT) for the financial support.

Appendix A. Supplementary data

CCDC 1041695 contain the supplementary crystallographic data for Mn(III)(Cl)L complex. These data can be obtained free of charge via http://www.ccdc.cam.ac.uk/conts/retrieving.html, or from the Cambridge Crystallographic Data Centre, 12 Union Road, Cambridge CB2 1EZ, UK; fax: (+44) 1223-336-033; or e-mail: deposit@ccdc.cam.ac.uk.

References

1 Hernndez-Molina R & Mederos A, *Comprehensive Coordination Chemistry II*, edited by J A McCleverty & T J Meyer, Eds Oxford Elsevier, 1 (2003) 411.
2 Sharma A K& Chandra S, *Spectrochim Acta A*, 78 (2011) 337.
3 Garnovskii A A, Nivorozhkin A L & Minkin V I, *Coord Chem Rev*, 126 (1993) 1.
4 Gupta K C & Sutar A K, *J Mol Catal A-Chem*, 272 (2007) 64.
5 (a) Deronzier A & Moutet J C, *Accounts Chem Res*, 22 (1989) 249; (b) Chaube V D, Shylesh S & Singh A P, *J Mol Catal A: Chem*, 241 (2005) 79; (c) Ourari A, Bougossa I, Bouacida S, Aggoun D, Ruiz-Rosas R, Morallon E & Merazig H, *J Iran Chem Soc*, 14 (2017) 703.
6 Tyagi P, Chandra S, Saraswat B S & Yadav D, *Spectrochim Acta Part A*, 145 (2015) 155.
7 Bougossa I, Aggoun D, Ourari A, Berenguer R, Bouacida S & Morallon E, *Chem Papers*, 74 (2020) 3825.
8 Mohamed R G, Elantabli F M, Helal N H & El-Medani S M, *Spectrochim Acta Part A*, 141 (2015) 316.
9 Swami B L & Ikram S, *Rev Adv Mater Sci*, 4 (2015) 239.
10 Church T L, GetzlerY D Y L & Coates G W, *J Am Chem Soc*, 31 (2006) 128.
11 Egekenze R, Gultneh Y &Butcher R, *Polyhedron*, 144 (2018) 198.
12 Serbest K, Özen A, Ünver Y, Er M, Degirmencioglu I & Sancak K, *J Mol Struct*, 922 (2009) 1.
13 (a) Yusuf T L, Oladipo S D, Zamisa S, Kumalo H M, Lawal I A, Lawal M M & Mabuba N, *ACS Omega*, 6 (2021) 13704; (b) Spiro T G, *Metal Ion Activation Dioxygen*, Wiley, New York (1980).
14 (a) Choi Y K, Park J K & Jeon S, *Electroanalysis*, 11 (1999) 134; (b) Gaillon L & Bedioui F, *J Mol Catal A*, 214 (2004) 91.
15 Sahu S & Goldberg D P, *J Am Chem Soc*, 138 (2016)11410.
16 Que L, *J Biol Inorg Chem*, 22 (2017) 171.
17 Nam W, *Acc Chem Res*, 40 (2007) 465.
18 Fukuzumi S, Lee Y M & Nam W, *Chem Cat Chem*, 10 (2018) 9.
19 Zhang W, Lai W & Cao R, *Chem Rev*,117 (2017) 3717.
20 Nastri F, Chino M, Maglio O, Bhagi-Damodaran A, Lu Y & Lombardi A, *Chem Soc Rev*, 45 (2016) 5020.
21 Hematian S, Garcia-Bosch I & Karlin K D, *Acc Chem Res*, 48 (2015) 2462.
22 Jasniewski A J & Que L, *Chem Rev*, 118 (2018) 2554.
23 (a)Moutet J C & Ourari A, *Electrochim Acta*, 42 (1997) 2525; (b) Moutet J C, Ouennoughi Y, Ourari A &Hamar-Thibault S, *Electrochim Acta*, 40 (1995) 1827.
24 Ourari A, Baameur L, Khan M A & Bouet G, *Electrochem Commun*, 10 (2008) 1736.
25 Altomare A, Burla M C, Camalli M, Cascarano G L, Giacovazzo C, Guagliardi A, Moliterni A G G, Polidori G &Spagna R, *J Appl Cryst*, 32 (1999) 115.
26 Sheldrick G M, *Acta Cryst*, A64 (2008) 112.
27 Farrugia L J, *J Appl Cryst*, 30 (1997) 565.
28 Farrugia L J, *J Appl Cryst*, 32 (1999) 837.
29 Becke A D, *J Chem Phys*, 98 (1993) 5648.
30 Lee C, Yang W & Parr R G, *Phys Rev*, 37 (1998) 785.
31 Miehlich B, Savin A, Stoll A & Preuss H, *Chem Phys Lett*, 157 (1989) 200.
32 Messasma Z, Ourari A, Mahdadi R, Houchi S, Aggoun D, Kherbache A &Bentouhami E, *J Mol Struct*, 1171 (2018) 672.
33 Ourari A, Baameur L, Bouacida S & Ouari K, *Acta Cryst E*, 68 (2012) 1760.
34 Maiti M, Sadhukhan D, Thakurta S, Zangrando E, Pilet G, Bauzá A, Frontera A, Dede B & Mitra S, *Polyhedron*, 75 (2014) 40.
35 Jeewoth T, Bhowon M G & Wah H L K, *Trans Met Chem*, 24 (1999) 445.
36 (a) Silverstein R M & Webster F X, *Spectrometric Identification of Organic Compounds*, 6th Edn, John Wiley and Sons, New York (1999) 34; (b) Droes R, Nardin G, Randaccio L, Siega P, Tauzher G &Vrdojak V, *InorgChim Acta*, 348 (2003) 239.
37 Turner M, Celik C, Koksal H & Serin S, *Trans Met Chem*, 24(1999) 525.
38 Boucher L G, *J InorgNucl Chem*, 36(1974) 531.
39 (a) Bellamy L J, *The Infrared Spectra of Complex Molecules*, 3rd Edn, Chapman and Hall, London (1975) 52; (b) Lever A B P, *Inorganic Electronic Spectroscopy*, 2nd Edn, Elsevier, London (1992).
40 (a) Etter M C, MacDonaldJ C & Bernstein J, *Acta Cryst B*, 46 (1990) 256; (b) Bernstein J, Davis R E, Shimoni L & Chang N L, *Angew Chem Int Ed Engl*, 34 (1995) 1555.
41 Hargittai M & Hargittai I, *Int J Quantum Chem*, 44 (1992) 1057.
42 Lawal M M, Govender T, Maguire G E, Kruger H G & Honarparvar B, *Int J Quantum Chem*, 118 (2018) 25497.
43 Zhan C G, Nichols J A & Dixon D A, *J Phys Chem A*, 107 (2003) 4184.
44 Liu S B, *J Chem Sci*, 117 (2005) 477.
45 Muthu S, Prasath M, Paulraj E I & Balaji R A, *Spectrochim Acta A*, 120 (2014) 185.
46 Klinger R J & Kochi J K, *J Phys Chem*, 85 (1981) 1731.
47 Sidir I, Sidir Y G, Kumalar M & Tasal E, *J Mol Struct*, 964 (2010) 134.

48 Barakat A, Al-Majid A M, Soliman S M, Mabkhot Y N, Ali M, Ghabbour H A, Fun H K & Wadood A, *Chem Central J*, 9 (2015) 1.
49 Yousef T A, *J Mol Struct*, 1215 (2020) 128180.
50 Densov J G, Makris T M, Sligar S G & Schlichting I, *Chem Rev*, 105 (2005) 2253.
51 Lundquist J T, Nicholson J R & Nicholson R S, *J Electroanal Chem*, 16 (1968) 445.
52 Ourari A, Ouari K, Bouet G & Khan M A, *J Coord Chem*, 61 (2008) 3846.
53 Cai C X, Xue K H, Xu X Y & Luo Q H, *J Appl Electrochem*, 27 (1997) 793.
54 Horwitz C P, Creager S E & Murray R W, *Inorg Chem*, 29 (1990) 1000.
55 Gunsalus I C, Pederson T C & Sligar S G, *Annu Rev Biochem*, 44 (1975) 377.
56 Ourari A, Ouari K, Moumeni W, Sibous L, Bouet G & Khan M A, *Trans Met Chem*, 31 (2006) 169.
57 Srinivasan K, Michaud P & Kochi J K, *J Am Chem Soc*, 108 (1986) 2309.
58 Kureshy R I, Khan N H, Abdi S H R, Iyer P & Bhatt A K, *J Mol Catal A-Chem*, 120 (1997) 101.
59 Samsel E G, Srinivasan K & Kochi J K, *J Am Chem Soc*, 107 (1985) 7606.